Elastic and inelastic scattering to low-lying states of ^{58}Ni and ^{90}Zr using 240-MeV ^{6}Li

Krishichayan, X. Chen,[*] Y.-W. Lui, Y. Tokimoto, J. Button, and D. H. Youngblood

Cyclotron Institute, Texas A&M University, College Station, Texas 77843, USA

(Received 10 October 2009; published 6 January 2010)

Elastic and inelastic scattering of 240-MeV ^{6}Li particles from ^{58}Ni and ^{90}Zr were measured with the multipole-dipole-multipole spectrometer from $4° \leqslant \theta_{\mathrm{c.m.}} \leqslant 43°$. The elastic scattering data were fitted with the double-folding model using the density-dependent M3Y NN effective interaction and with a phenomenological Woods-Saxon potential. $B(E2)$ and $B(E3)$ values obtained for low-lying 2^+ and 3^- states with the double-folding calculations agreed with the adopted values.

I. INTRODUCTION

The inelastic scattering of α particles has been a valuable technique for studying isoscalar giant monopole resonances (ISGMR) for many years [1–3]. A comparison of the results of systematic studies of the ISGMR in stable nuclei with calculations using the Gogny interaction resulted in the value $K_{\mathrm{nm}} = 231 \pm 5$ MeV [1]. Calculations with other interactions and relativistic models have shown that the location of the giant monopole resonance (GMR) is also sensitive to the symmetry energy, and studies of stable Sn isotopes have led to some constraints on K_{sym} [4,5]. To determine the contribution from symmetry energy more accurately, a systematic study of the ISGMR over a wide range of $(N–Z)/A$ is necessary. This range can be expanded by extending ISGMR measurements to unstable nuclei using inverse reactions. Using beams of 240-MeV [1] and 400-MeV [6] α particles, the peak cross sections for the monopole resonance have been shown to approach 0.5 b/sr, sufficient to observe these resonances with low-intensity rare isotope beams in inverse reactions. Unfortunately He targets have serious limitations for such studies. At Riken a liquid He target 120 mg/cm^2 in thickness was employed to study the ISGMR in ^{14}O [7] using 60 MeV/nucleon ^{14}O beams. However, the energy straggling in such a target is large, and for heavier mass projectiles, it would be unacceptably large. The excitation of the GMR in the ^{56}Ni nucleus [8] has also been reported using deuterium in the active target MAYA at the Grand Accelerateur National D'Ions Lourds (GANIL) [9].

^{6}Li is an isoscalar projectile ($N = Z$), and it has been shown that the inelastic scattering of ^{6}Li excites the ISGMR strongly [10]. For ^{6}Li scattering, the low-lying particle emission threshold gives a large breakup probability into the dominant channel ^{6}Li $\rightarrow \alpha + d$. Therefore the contribution of multistep processes should be low especially at higher excitation energy.

To study the ISGMR in unstable nuclei with inelastic scattering using a ^{6}Li target, optical parameters are needed for distorted-wave Born approximation (DWBA) calculations of multipole excitations. Therefore we are using a ^{6}Li beam on

stable targets to investigate optical potentials and explore how reliable $B(E2)$ and $B(E3)$ values for well-known low-lying states are reproduced. Beene *et al.* [11] have shown that $B(EL)$ values in agreement with electromagnetic values can be obtained from hadron inelastic scattering using the folding model, but that $B(EL)$ values obtained using Woods-Saxon (WS) potentials can have systematic and large differences from those obtained from electromagnetic reactions. Our primary focus is to obtain appropriate folding model parameters that eventually can be used to obtain a systematic parameter set that can be applied to studies with unstable nuclei.

The double-folding model has been successfully [12–14] used for heavy-ion scattering studies. However, for the scattering of weakly bound nuclei such as ^{6}Li, ^{7}Li, and ^{9}Be [12], the elastic data require a renormalization (N_r) of the real folded potential with a factor around 0.5–0.6. The reason for this anomalous behavior of N_r is that the loosely bound nuclei are very easy to break up, which is otherwise not accounted for in the folding model. This effect can be represented [14] by a complex dynamical polarization potential (DPP) that has a strongly repulsive real part. Sakuragi [15] has thoroughly investigated the breakup effect of the projectile using coupled discretized continuum channels (CDCC) technique and confirmed that the elastic scattering data could be fitted well with the N_r close to unity when coupling to the breakup channel was included.

There have been several previous studies of elastic and inelastic scattering of ^{6}Li ions from various targets. Chen *et al.* [10,16,17] studied elastic and inelastic scattering of 240-MeV ^{6}Li from ^{24}Mg, ^{28}Si, and ^{116}Sn and investigated double-folding calculations using several NN interactions, obtaining $B(EL)$ values in agreement with electromagnetic results for low-lying states and getting general agreement with giant resonance distributions obtained with α particles. Nadasen *et al.* [18,19] have studied ^{6}Li elastic scattering from ^{12}C, ^{28}Si, ^{40}Ca, ^{58}Ni, ^{90}Zr, and ^{208}Pb at 210 MeV but fit the data only with WS potentials. In another study, Nadasen *et al.* [20] scattered 318-MeV ^{6}Li ions from ^{12}C and ^{28}Si and fit this data with both phenomenological and double-folding potentials. The same group studied inelastic scattering of 210-MeV ^{6}Li ions from low-lying 2^+ states in ^{12}C, ^{28}Si, and ^{58}Ni [21] and obtained quadrupole moments in agreement with those measured with electromagnetic interactions. A study of

_____

*Present address: Department of Chemistry, Washington University at St. Louis, St. Louis, MO 63130, USA.

600-MeV ^{6}Li scattering on ^{12}C, ^{58}Ni, ^{90}Zr, and ^{208}Pb targets [22] that investigated the coupling effect between the elastic and the breakup channels at intermediate energy was reported in 2000.

In this work, 240-MeV ^{6}Li elastic scattering on ^{58}Ni and ^{90}Zr was carried out and optical potentials obtained with the double folding were used to fit the data. For comparison with the other investigations of ^{6}Li scattering described above, we also carried out calculations with Woods-Saxon potentials. The differential cross sections for the low-lying 2^+ and 3^- states were also extracted from the experiment and DWBA calculations were carried out, which provides another test of the potentials as well as information on the validity of collective form factors normally used to describe the excitation of these states. The best-fit values for $B(EL)$ with both the models were extracted. Differential cross sections for the excitation of giant resonances in these nuclei were also calculated using the double-folding model.

II. EXPERIMENTAL TECHNIQUE

The experimental technique for the ^{6}Li scattering measurements was similar to that for α scattering that has been described in Ref. [23] and is summarized briefly below.

Beams of 240-MeV ^{6}Li ions from the Texas A&M K500 superconducting cyclotron bombarded self-supporting target foils (enriched to more than 95%, 4.0 mg/cm^2 ^{58}Ni and 5.0 mg/cm^2 ^{90}Zr) in the target chamber of the multipole-dipole-multipole (MDM) spectrometer [24]. The beam was delivered to the MDM spectrometer through a beam analysis system [25] to remove halo and improve momentum resolution and was stopped on a Faraday cup inside the scattering chamber. The horizontal acceptance of the spectrometer was 4° and ray tracing was used to reconstruct the scattering angle. The focal-plane detector consisted of four 60-cm-long resistive wire proportional counters to measure position, an ionization chamber to measure ΔE, and a scintillator to measure E and to provide a fast timing signal for each event. The out-of-plane scattering angle (ϕ) was not measured. The principles of operation of the detector are similar to those of the detector described in Ref. [26]. The details of angle and position calibrations are described in Ref. [27]. A position resolution of approximately 0.9 mm and a scattering angle resolution of about 0.09° were obtained.

Data for elastic scattering and inelastic scattering exciting the low-lying states were taken at spectrometer angles ranging from 4° to 43° with a spectrometer acceptance of $\Delta\theta = 4.0^\circ$. The vertical acceptance was $\pm1^\circ$ for spectrometer angles from 4° to 9° and $\pm2^\circ$ for spectrometer angles from 11° to 43°. In the data analysis, data taken at one spectrometer angle were divided into ten angle bins, each angle bin corresponding to $\Delta\theta \approx 0.4^\circ$. The average angle for each bin was determined by averaging over the height of the solid angle defining slit and the width of the angle bin. For each angle bin, the elastic and inelastic scattering peak positions, widths, and cross sections were extracted by integration or by a
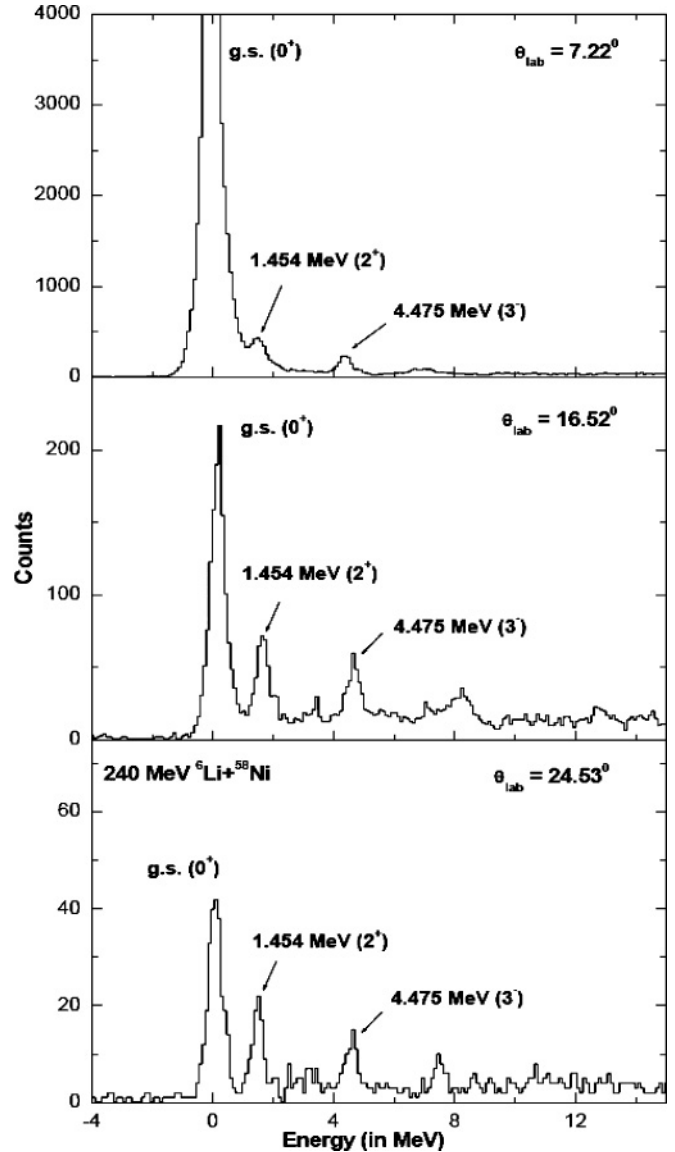

FIG. 1. Representative energy spectra for the scattering of 240-MeV ^{6}Li ions from ^{58}Ni at $\theta_{\text{lab}} = 7.22^\circ$, 16.52°, and 24.53°, showing the elastic and 2^+ and 3^- low-lying states.

Gaussian fitting routine. The target thicknesses were obtained by measuring the energy loss of the 240-MeV α beam passing through the targets. The absolute differential cross section for each angle bin was obtained from the combination of yield, charge integration, target thickness, solid angle, and dead time correction. The cumulative uncertainties in target thickness, solid angle, etc., result in a $\pm10\%$ uncertainty in cross section. Data from a monitor detector, fixed at $\theta_{\text{lab}} = 25^\circ$, were used as a check on the charge integration to verify the normalization between the different data sets across the angular range.

Figure 1 shows representative energy spectra obtained with the ^{58}Ni target at $\theta_{\text{lab}} = 7.22^\circ$, 16.52°, and 24.53°. As is clear from the spectra, the 2^+ and 3^- low-lying states are well separated from the ground-state peak (elastic peak). Experimental angular distributions of the cross section
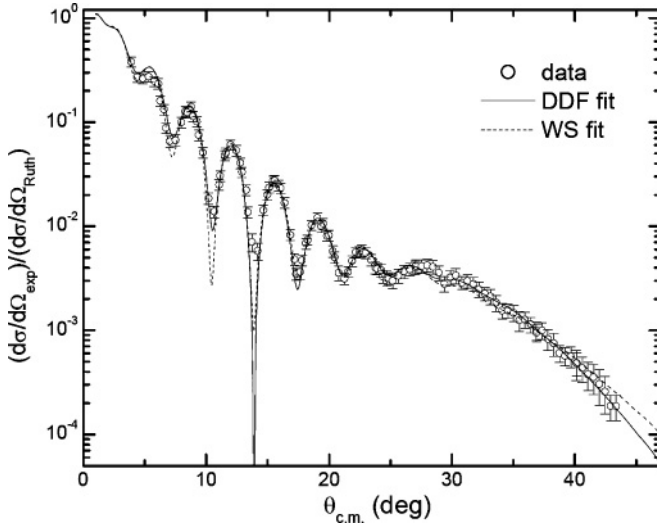
FIG. 2. Experimental angular distribution of the cross section (relative to the Rutherford cross section) and fits for ^{6}Li + ^{58}Ni elastic scattering using WS potential and DDF potential parameters are shown. The error bars include statistical and systematic errors.

(relative to the Rutherford cross section) for elastic scattering data are shown in Figs. 2 and 3.

III. RESULTS AND ANALYSIS

A. Optical model and parametrization of the elastic scattering data

The elastic scattering data were fit with optical model calculations using the program ECIS [28] with a WS phenomenological potential of the form

$$U(r) = -V_0 \{1/[1 + \exp((r - R_V)/a)]\}$$
$$\quad - i W_0 \{1/[1 + \exp((r - R_W)/a)]\} + V_C(r) \quad (1)$$

$$R_V = r_0(A_T^{1/3} + A_P^{1/3}), \quad R_W = r_{i0}(A_T^{1/3} + A_P^{1/3}), \quad (2)$$

where A_T is the mass number of the target and A_P is the mass number of projectile.

The quality of fit of elastic as well as inelastic scattering is estimated by χ^2, defined by

$$\chi^2 = \frac{1}{N} \sum_{i=1}^{N} \left[\frac{\sigma(\theta_i)^{\text{cal}} - \sigma(\theta_i)^{\text{exp}}}{\Delta\sigma(\theta_i)} \right]^2, \quad (3)$$
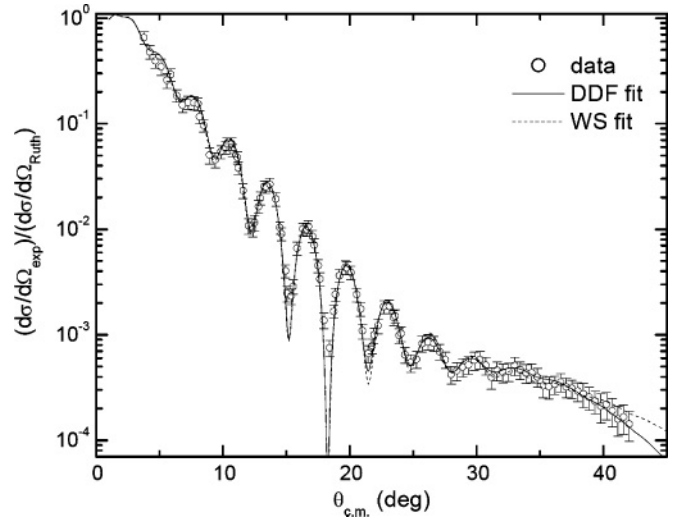

FIG. 3. Same as Fig. 2, but for the ^{90}Zr target.

where N is the number of data points, $\sigma(\theta_i)^{\text{cal}}$ is the ith calculated cross section, $\sigma(\theta_i)^{\text{exp}}$ is the experimental cross section, and $\Delta\sigma(\theta_i)$ is the corresponding absolute uncertainty.

The optical potential parameters that best describe the elastic scattering of ^{6}Li on ^{58}Ni and ^{90}Zr are listed in Table I. The calculated angular distributions for the ratio between calculated cross sections and Rutherford cross sections are shown in Figs. 2 and 3. As can be seen, the measured angular distributions are reasonably well described by the calculations. Parameters obtained by Nadasen *et al.* [18,19] and Farid and Hassanain [29] using 210-MeV ^{6}Li are also shown in Table I for comparison.

B. Double-folding model description of the elastic scattering data

A microscopic understanding of light heavy-ion scattering can be obtained if one relates the optical potential to a fundamental nucleon-nucleon (NN) interaction by folding this interaction with the nuclear matter distributions of both the target and the projectile nuclei [12].

In a simple picture, the nucleus-nucleus optical potential in this double-folding (DF) model is obtained from

$$V^{\text{DF}}(R) = \iint \rho_1(r_1)\rho_2(r_2)v_{nn}(s, \rho_1, \rho_2)d\vec{r}_1 d\vec{r}_2, \quad (4)$$

where $\rho_1(r_1)$ and $\rho_2(r_2)$ are the nuclear matter distributions for projectile and target nuclei, respectively, and $v_{nn}(s)$ is

TABLE I. Optical parameters obtained from the analysis of ^{6}Li scattering, using Woods-Saxon (WS) geometry, as described in the text. The asterisk means that $R_{v(w)} = r_{0(i0)}A_T^{1/3}$.

E_{Li} (MeV)	Target	V (MeV)	r_0 (fm)	a (fm)	W (MeV)	r_{i0} (fm)	a_i (fm)	J_v (MeV fm^3)	J_w (MeV fm^3)	χ^2	σ_r (mb)
240 [Present]	^{58}Ni	160.37	0.785	0.926	33.08	1.070	0.899	245	109	0.98	2187
210 [18,29]		174.50	1.136*	0.907	32.00	1.607*	0.806	254	108	6.20	2078
240 [Present]	^{90}Zr	159.67	0.873	0.823	38.61	1.075	0.949	252	111	1.22	2709
210 [19,29]		170.00	1.182*	0.939	31.30	1.627*	0.810	257	106	8.30	2618

TABLE II. Parameters for the Fermi model [Eq. (5)] of the ground-state density distributions.

Nucleus	ρ_0 (fm^{-3})	c (fm)	a (fm)	$\langle r^2 \rangle$ (fm)	Reference
^{58}Ni	0.176	4.08	0.515	3.695	[32]
^{90}Zr	0.165	4.90	0.515	4.251	[29]

the effective NN interaction with $s = |\vec{R} - \vec{r}_1 + \vec{r}_2|$. The key inputs in a folding calculation are the nuclear densities of the interacting nuclei and the effective NN interaction.

There are several nucleon-nucleon effective interactions that have been used in folding model calculations. In the present work, the Paris version of M3Y NN interaction was used to carry out density-dependent double-folding calculations. Details of this interaction can be found in Refs. [10,16,30].

Satchler and Khoa [31,32] found that better fits to the measurements taken at angles beyond the Fraunhofer diffraction region were obtained by a hybrid model in which the real interaction was obtained with folding and the imaginary part was represented by a Woods-Saxon potential. So, in the present work, only the real parts of the optical potentials were obtained by folding. Density-dependent double-folding (DDF) calculations were carried out with the folding code DFPD4 [32].

The ground-state density of the projectile ^{6}Li was obtained from proton scattering with the cluster-orbital shell-model approximation (COSMA) [33] and the Fermi model,

$$\rho_T(r) = \frac{\rho_0}{[1 + \exp((r - c)/a)]} \text{fm}^{-3}, \quad (5)$$

was used for ^{58}Ni and ^{90}Zr target nuclei densities. The density parameters used in the folding model calculations are listed in Table II.

The optical potential parameters obtained from the density-dependent double-folding calculations (Paris M3Y interaction) are listed in Table III and the calculated angular distributions of the cross sections are plotted along with elastic scattering data in Figs. 2 and 3. The renormalization factors (N_r) obtained are around 0.87 for both ^{58}Ni and ^{90}Zr target nuclei. Similar values, 0.823 and 0.887, have been reported
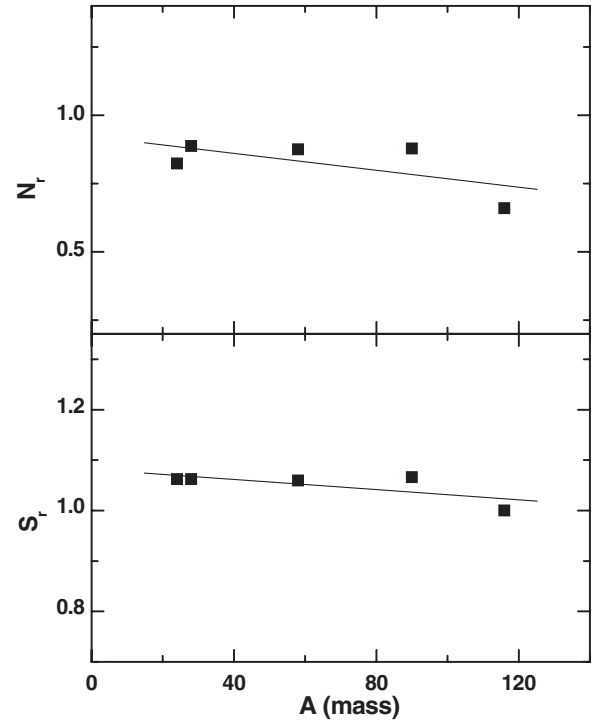

FIG. 4. The target mass number dependence of real normalization (N_r) and radius scaling (S_r) factors is shown by solid squares. The ^{24}Mg and ^{28}Si results are from Ref. [16], and the ^{116}Sn result is from Ref. [17]. Solid lines are linear fits of the data.

by X. Chen *et al.* [16] for ^{24}Mg and ^{28}Si, respectively, using the same interaction. A somewhat lower value $N_r = 0.65$ was required to fit 240-MeV ^{6}Li scattering from ^{116}Sn [17]. Farid and Hassanain [29,34] have analyzed 210-MeV ^{6}Li scattering from ^{58}Ni and ^{90}Zr using double-folding calculations with density-independent M3Y and JLM NN interactions. In both cases the renormalization factors (N_r) are lower (see Table I) than our results with the density-dependent M3Y NN interaction. The target mass number dependence of N_r values obtained for 240-MeV ^{6}Li scattering is illustrated in Fig. 4. Except for ^{116}Sn, N_r is almost the same ($\sim$0.87) for the nuclei (^{24}Mg, ^{28}Si, ^{58}Ni, and ^{90}Zr) studied.

A scaling factor, S_r, on the radius of the real optical potential is necessary to fit the elastic scattering data for both ^{58}Ni and

TABLE III. Optical model parameters obtained from fits of elastic scattering with the density-dependent double-folding (DDF) calculations using the M3Y interaction. N_r is the renormalization factor for the real potential. S_r is the scaling factor for the radius of the real potential. W, r_{i0}, and a_i are WS parameters for the imaginary potentials. J_v and J_w are the volume integral per nucleon pair for the real and imaginary potentials, respectively. σ_r is the total cross section of the reaction. DIF means density-independent folded potential. The asterisk means that $R_{v(w)} = r_{0(i0)} A_T^{1/3}$.

Target	E_{Li} (MeV)	NN int.	Potential type	N_r	S_r	W (MeV)	r_{i0} (fm)	a_i (fm)	J_v (MeV fm^3)	J_w (MeV fm^3)	χ^2	σ_r (mb)
^{58}Ni	240 [Present]	M3Y	DDF	0.875	1.059	35.33	1.027	1.057	244.6	112.0	0.9	2397
	210 [29]	M3Y	DIF	0.640		26.20	1.673*	0.767	237.0	97.0	6.1	2061
	210 [34]	JLM	DIF	0.408		19.27	1.776*	0.820	195.0		28.1	2204
^{90}Zr	240 [Present]	M3Y	DDF	0.878	1.066	33.34	1.090	1.006	239.5	101.5	1.1	2792
	210 [29]	M3Y	DIF	0.700		31.30	1.596*	0.917	263.0	103.0	4.9	2744
	210 [34]	JLM	DIF	0.448		25.43	1.673*	0.847	217.0		10.5	2695

^{90}Zr. A similar scaling factor was required to fit data for ^{6}Li scattering from ^{24}Mg and ^{28}Si target nuclei [16], which has been attributed to a repulsive surface correction for dynamical polarization potential (DPP) [16,35]. As is clear from Fig. 4, the value of S_r is almost constant and independent of the target mass number.

The volume integrals of the optical potentials per interacting nucleon pair were determined by the relations

$$J_v = \frac{1}{A_T A_P} \int v(r) d\tau,$$
$$J_w = \frac{1}{A_T A_P} \int w(r) d\tau, \quad (6)$$

where $v(r)$ and $w(r)$ are the real and imaginary parts of the optical potential and A_T and A_P are the mass numbers of the target and the projectile. It has been suggested [13,14] that the volume integral of the nuclear potential is better determined by the data than the potential itself. According to Brandan and Satchler [14], even in the cases of extreme sensitivity of the scattering to the potential, a small readjustment of the various parameters is possible, while keeping the volume integral a constant. This fact might be exploited to better understand the optical potential parameters for light heavy-ions like ^{6}Li.

Volume integrals of the real and imaginary parts of optical potentials are both energy and target mass dependent. According to Gupta and Murthy [36], the value of the volume integral of the real part of the optical potential will slowly decrease as the incident energy and target mass increases. Such energy and mass dependence was further explored by Nadasen *et al.* [19] using 210-MeV ^{6}Li scattering on ^{12}C, ^{28}Si, ^{40}Ca, ^{58}Ni, and ^{90}Zr. They suggested that the volume integrals, derived using a WS phenomenological form factor, depend on $A^{-1/3}$, in the form of (using the least-square fit to the data [19])

$$J_R/6A = J_0(1 + CA^{-1/3}),$$
$$J_W/6A = J_0'(1 + C'A^{-1/3}), \quad (7)$$

for real and imaginary parts of the optical potential, respectively, with $J_0 \approx 215$ MeV fm^3, $J_0' \approx 45$ MeV fm^3, $C \approx 0.88$, and $C' \approx 5.9$. These are compared with those obtained in the present experiment using both WS and double folding approaches in Fig. 5. The values of volume integrals of the real and imaginary parts of the optical potentials obtained with the WS potential model are almost comparable for 210- and 240-MeV ^{6}Li data. The corresponding values obtained with the double-folding model are also close except for the integral of the real potential for ^{116}Sn. The values of volume integrals of the real parts of the optical potentials obtained with WS form factors for ^{58}Ni and ^{90}Zr are in reasonable agreement with those predicted using the energy dependencies prescribed by Nadasen *et al.* [19] and Gupta and Murthy [36].

C. Low-lying states and calculations for giant resonances

The angular distributions for the 2^+ and 3^- states of ^{58}Ni (at 1.454 and 4.475 MeV, respectively) and ^{90}Zr (at 2.186
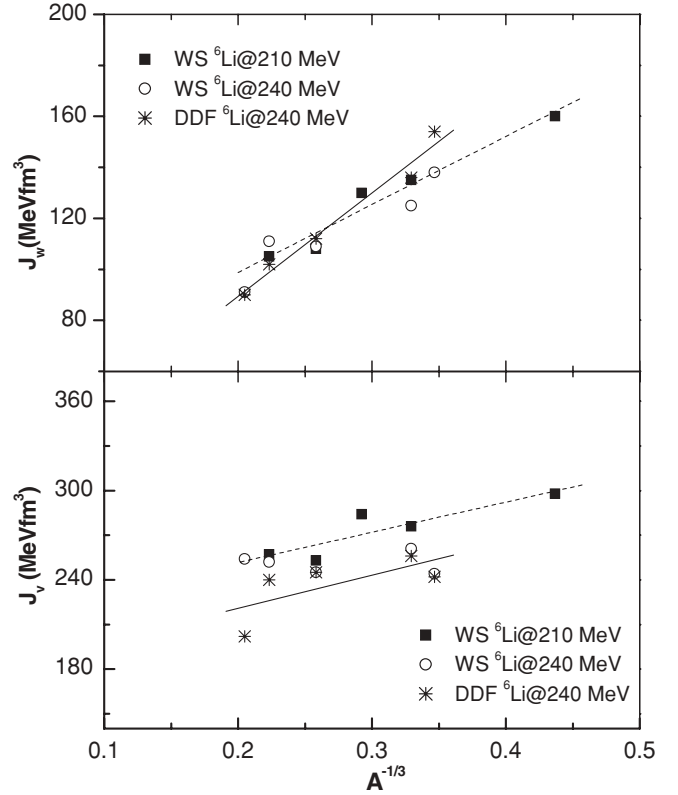

FIG. 5. Plot of the real and imaginary volume integrals obtained from 240-MeV data are compared with those obtained from 210-MeV data by Nadasen *et al.* [19] using WS form factors. The ^{24}Mg and ^{28}Si results are from Ref. [16], and the ^{116}Sn results are from Ref. [17]. The solid and broken lines are linear fits of the data from the present work and from Nadasen *et al.*, respectively. The solid squares show Nadasen *et al.*'s results, while the circles show our results using WS form factors. The asterisks show our results using double folding.

and 2.747 MeV, respectively) are shown in Figs. 6 and 7. As a further test of the optical model parameters obtained from elastic scattering, these distributions were compared to DWBA calculations using the deformed potential model as well as the double-folding model. The double-folding model was also used for calculations of the excitation of nuclear giant resonances.

1. Deformed potential model

The transition potential (both real and imaginary) used to describe inelastic scattering to excited states of the target nucleus is directly obtained as the derivative of the WS potential $U(r)$ for $l \geqslant 2$:

$$G_l^{\text{DP}}(r) = -\delta_l^U \frac{dU(r)}{dr}, \quad (8)$$

where δ_l^U is the potential deformation length. The values of deformation parameters δ_l and α_0 are related to sum-rule limits as discussed in Ref. [10].
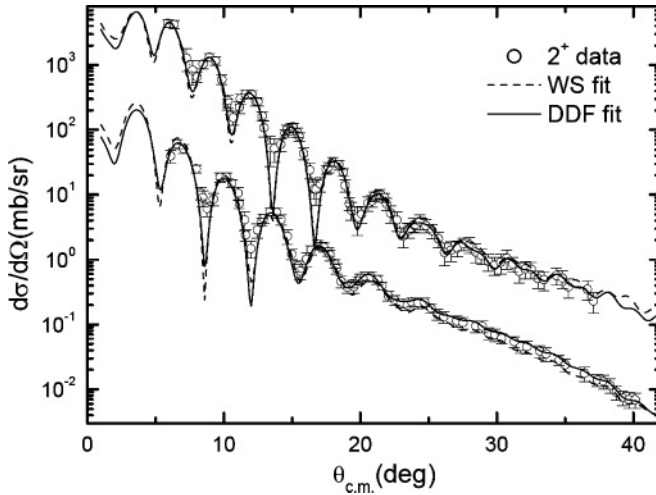
FIG. 6. The angular distributions of the differential cross sections calculated with deformed potential model and folding models for inelastic scattering to the 1.454-MeV 2^+ state of ^{58}Ni and the 2.186-MeV 2^+ state of ^{90}Zr are plotted along with the data points. The $B(E2)$ values used for DP and DDF models calculations are best-fit values shown in Table IV. The error bars represent statistical and systematic errors.

2. Double-folding model

In the folding model approach, the transition potential can be expressed as

$$G_l^{\mathrm{DF}}(r) = \int g_l(r_2)\bar{v}_l(r_1, r_2)r_2^2 dr_2, \qquad (9)$$

where $g_l(r_2)$ is the transition density for a 2^l-pole excitation of the target and $\bar{v}_l(r_1, r_2)$ is the 2^l-pole component of an
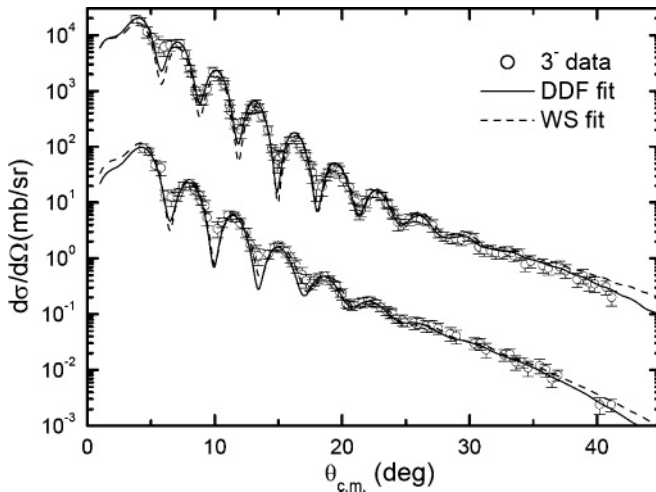

FIG. 7. The differential cross sections calculated with deformed potential model and folding models for inelastic scattering to the 4.475-MeV 3^- state of ^{58}Ni and 2.747-MeV 3^- state of ^{90}Zr are plotted along with the data points versus average center-of-mass angle. The $B(E3)$ values used for DP and DDF models calculations are listed in Table IV. The error bars represent statistical and systematic errors.

effective nucleon-nucleon interaction, $v_{nn}(s)$, averaged over the ground-state projectile density distribution $\rho_1(r)$. Detailed information on the folding model approach including exchange terms can be found in Refs. [13,32].

Following the discussion in Ref. [13], the transition density for $l \geqslant 2$ can be expressed as

$$g_l(r) = -\delta_l^m \frac{d\rho(r)}{dr}, \quad l \geqslant 2, \qquad (10)$$

where $\rho(r)$ is the ground-state density distribution of the excited nucleus and δ_l^m is the corresponding matter deformation length that provides a measure of the strength of transition.

The transition density for a monopole resonance ($l = 0$) can be obtained with a simple scaling on radius [13,37],

$$g_0(r) = -\alpha_0^m \left[3\rho(r) + r\frac{d\rho(r)}{dr} \right]. \qquad (11)$$

The transition density for isoscalar dipole excitation ($l = 1$) is given as [38]

$$g_1(r) = -\frac{\beta_1}{c\sqrt{3}} \left[3r^2 \frac{d}{dr} + 10r - \frac{5}{3}\langle r^2 \rangle \frac{d}{dr} + \varepsilon \left(r\frac{d^2}{dr^2} + 4\frac{d}{dr} \right) \right] \rho(r), \qquad (12)$$

where c is the half density radius of the Fermi mass distribution. The transition density given above (12) is only for one of the magnetic substates and must be multiplied by $(2l + 1)^{1/2}$ to represent excitation of the ISGDR [39].

The real parts of the transition potentials were calculated by folding the NN effective interaction over the densities of the target and the projectile, while the imaginary parts were constructed with the deformed potential model. The transition potentials were calculated with DFPD4 [32] and the cross sections were calculated with ECIS [28]. The mass deformation parameters for the 2^+ and 3^- states were obtained from electromagnetic $B(EL)$ values by assuming that the mass and Coulomb deformation lengths are the same. The calculated angular distributions of the cross section for the 2^+ and 3^- states in ^{58}Ni and ^{90}Zr are shown in Figs. 6 and 7, respectively, normalized to the data to produce the lowest χ^2.

$B(EL)$ values obtained from the fits are listed in Table IV. There are two errors given for each fitted $B(EL)$ value. The superscript represents statistical error, which comes from the fit of inelastic scattering cross sections. The subscript error represents the total error including both statistical and systematic errors (and the error in the absolute cross section).

The results are compared with $B(EL)$ values obtained using electron scattering [40,41] and also are compared with the adopted $B(E2)$ [42] and $B(E3)$ [43] values in Table IV. The $B(E2)$ and $B(E3)$ values for the 2^+ and 3^- states in ^{58}Ni and ^{90}Zr obtained with the double-folding calculations agree with the adopted values and with the values from electron scattering. The $B(EL)$ values obtained from the deformed potential model for the 2^+ states are in agreement with the adopted values, but those obtained for the 3^- states in this work are much lower than the adopted values. This is consistent with

TABLE IV. $B(EL)$ values for 2^+ and 3^- states of ^{58}Ni and ^{90}Zr obtained with the deformed potential model and the double-folding model. Adopted values of $B(E2)$ and $B(E3)$, as well as values extracted from electron scattering, are shown in the table. For $B(EL)$ values obtained from ^{6}Li scattering, the superscript errors represent statistical errors, while the subscript errors represent total errors including statistical and systematic errors. DP is deformed potential, DDF is density-dependent double folding, and EM is electromagnetic.

Work	Model	$B(E2)$ $(e^2\,b^2)$	$B(E3)$ $(e^2\,b^3)$
^{58}Ni		$J^\pi = 2^+,$ $E_x = 1.454\,\text{MeV}$	$J^\pi = 3^-,$ $E_x = 4.475\,\text{MeV}$
Present	DP	$0.0728^{\pm0.0022}_{\pm0.0073}$	$0.0131^{\pm0.0004}_{\pm0.0013}$
	DDF	$0.0662^{\pm0.002}_{\pm0.007}$	$0.0160^{\pm0.0006}_{\pm0.0016}$
Electron scattering [40]	EM	0.0588 ± 0.004	0.0191 ± 0.0008
	Adopted value	0.0695 ± 0.002 [42]	0.0176 ± 0.0016 [43]
^{90}Zr		$J^\pi = 2^+,$ $E_x = 2.186\,\text{MeV}$	$J^\pi = 3^-,$ $E_x = 2.747\,\text{MeV}$
Present	DP	$0.055^{\pm0.002}_{\pm0.005}$	$0.053^{\pm0.002}_{\pm0.005}$
	DDF	$0.059^{\pm0.002}_{\pm0.006}$	$0.086^{\pm0.002}_{\pm0.009}$
Electron scattering [41]	EM	0.067 ± 0.006	0.0874 ± 0.01
	Adopted value	0.061 ± 0.004 [42]	0.098 ± 0.005 [43]

Beene *et al.*'s [11] conclusion that inelastic scattering analyzed with deformed potential model calculations do not reproduce electromagnetic transition probabilities. The inability of the deformed potential model to reproduce the strength of giant resonances, using ^{6}Li scattering, has been reported in Ref. [10], even though the deformed potential model gives fits to the elastic data and low-lying states comparable to those from the double-folding model.

Figures 8 and 9 show calculated differential cross sections for the excitation of various giant resonances ($l = 0$ to 3) in ^{58}Ni and ^{90}Zr, respectively, using the potential parameters obtained from the double-folding model. The calculations were done for resonances at $E_x = 18$ and 17 MeV, respectively, in ^{58}Ni and ^{90}Zr using ECIS [28], assuming that these resonances exhaust 100% of the respective EWSRs. The peak

cross sections for the monopole resonances at $0°$ in these nuclei are found to be somewhat less than ^{116}Sn [10], but are adequate for studies with unstable beams. The ISGMR cross section decreases rapidly beyond $1°$, whereas the other multipoles are basically flat or slowly varying, so that ISGMR strength should be separable from the other multipoles.

IV. SUMMARY

Elastic and inelastic scattering of 240-MeV ^{6}Li particles from ^{58}Ni and ^{90}Zr were measured with the MDM spectrometer. Optical parameters were obtained from the fit of elastic scattering data using double folding with the density-dependent M3Y NN interaction as well as the WS
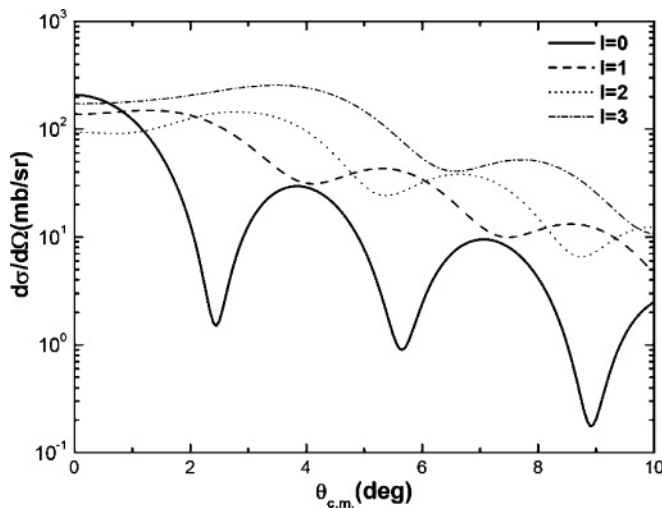

FIG. 8. Angular distributions of the differential cross section for 240-MeV ^{6}Li inelastic scattering from ^{58}Ni for $l = 0$–3 for 100% of the EWSR at $E_x = 18$ MeV.
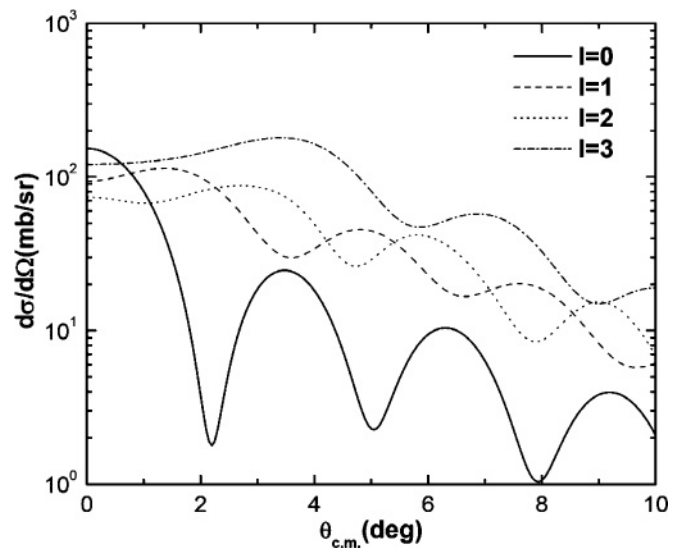

FIG. 9. Angular distributions of the differential cross section for 240-MeV ^{6}Li inelastic scattering from ^{90}Zr for $l = 0$–3 for 100% of the EWSR at $E_x = 17$ MeV.

phenomenological potential. $B(EL)$ values obtained with the double-folding model agree well with adopted values. Volume integrals of the real and imaginary parts of the optical potentials were obtained and are in reasonable agreement with those obtained at 210 MeV using Woods-Saxon potentials.

[1] D. H. Youngblood, H. L. Clark, and Y.-W. Lui, Phys. Rev. Lett. **82**, 691 (1999).

[2] D. H. Youngblood, Y.-W. Lui, B. John, Y. Tokimoto, H. L. Clark, and X. Chen, Phys. Rev. C **69**, 054312 (2004).

[3] T. Li *et al.*, Phys. Rev. Lett. **99**, 162503 (2007).

[4] S. Shlomo, V. Kolomietz, and G. Colò, Eur. Phys. J. A **30**, 23 (2006); H. Sagawa, S. Yoshida, G.-M. Zeng, J.-Z. Gu, and X.-Z. Zhang, Phys. Rev. C **76**, 034327 (2007); M. Centelles, X. Roca-Maza, X. Vinas, and M. Warda, Phys. Rev. Lett. **102**, 122502 (2009).

[5] J. Piekarewicz, Phys. Rev. C **66**, 034305 (2002); **76**, 031301(R) (2007).

[6] M. Uchida *et al.*, Phys. Lett. **B557**, 12 (2003).

[7] H. Baba *et al.*, Nucl. Phys. **A788**, 188 (2007).

[8] C. Monrozeau *et al.*, Nucl. Phys. **A788**, 182 (2007); C. Monrozeau *et al.*, Phys. Rev. Lett. **100**, 042501 (2008).

[9] C. E. Demonchy, Thesis T 03 06, Université Caen, France, 2003.

[10] X. Chen, Y.-W. Lui, H. L. Clark, Y. Tokimoto, and D. H. Youngblood, Phys. Rev. C **79**, 024320 (2009).

[11] J. R. Beene, D. J. Horen, and G. R. Stachler, Phys. Lett. **B344**, 67 (1995); Phys. Rev. C **48**, 3128 (1993).

[12] G. R. Satchler and W. G. Love, Phys. Rep. **55**, 183 (1979).

[13] G. R. Satchler, *Direct Nuclear Reactions* (Oxford University Press, New York, 1983).

[14] M. Brandan and G. R. Satchler, Phys. Rep. **285**, 143 (1997), and references therein.

[15] Y. Sakuragi, Phys. Rev. C **35**, 2161 (1987).

[16] X. Chen, Y.-W. Lui, H. L. Clark, Y. Tokimoto, and D. H. Youngblood, Phys. Rev. C **80**, 014312 (2009).

[17] X. Chen, Y.-W. Lui, H. L. Clark, Y. Tokimoto, and D. H. Youngblood, Phys. Rev. C **76**, 054606 (2007).

[18] A. Nadasen *et al.*, Phys. Rev. C **37**, 132 (1988).

[19] A. Nadasen, M. McMaster, M. Fingal, J. Tavormina, P. Schwandt, J. S. Winfield, M. F. Mohar, F. D. Becchetti, J. W. Jänecke, and R. E. Warner, Phys. Rev. C **39**, 536 (1989).

[20] A. Nadasen, T. Stevens, J. Farhat, J. Brusoe, P. Schwandt, J. S. Winfield, G. Yoo, N. Anantaraman, F. D. Becchetti, J. Brown *et al.*, Phys. Rev. C **47**, 674 (1993).

[21] A. Nadasen, M. McMaster, M. Fingal, J. Tavormina, J. S. Winfield, R. M. Ronningen, P. Schwandt, F. D. Becchetti, J. W. Jänecke, and R. E. Warner, Phys. Rev. C **40**, 1237 (1989).

[22] K. Schwarz *et al.*, Eur. Phys. J. A **7**, 367 (2000).

[23] D. H. Youngblood, Y.-W. Lui, and H. L. Clark, Phys. Rev. C **60**, 014304 (1999).

[24] D. M. Pringle, W. N. Catford, J. S. Winfield, D. G. Lewis, N. A. Jelley, K. W. Allen, and J. H. Coupland, Nucl. Instrum. Methods Phys. Res. A **245**, 230 (1986).

[25] D. H. Youngblood and J. D. Bronson, Nucl. Instrum. Methods Phys. Res. A **361**, 37 (1995).

[26] D. H. Youngblood, Y.-W. Lui, H. L. Clark, P. Oliver, and G. Simler, Nucl. Instrum. Methods Phys. Res. A **361**, 539 (1995).

[27] D. H. Youngblood, Y.-W. Lui, and H. L. Clark, Phys. Rev. C **55**, 2811 (1997).

[28] J. Raynal, ECIS code (unpublished); J. Raynal, Proceedings of the Workshop on Applied Nuclear Theory and Nuclear Model Calculations for Nuclear Technology Application, Trieste, Italy, 1988.

[29] M. El-Azab Farid and M. A. Hassanain, Nucl. Phys. **A678**, 39 (2000).

[30] M. Lacombe, B. Loiseau, J. M. Richard, R. Vinh Mau, J. Côté, P. Pirès, and R. de Tourreil, Phys. Rev. C **21**, 861 (1980).

[31] G. R. Satchler and D. T. Khoa, Phys. Rev. C **55**, 285 (1997).

[32] D. T. Khoa and G. R. Satchler, Nucl. Phys. **A668**, 3 (2000).

[33] A. A. Korsheninnikov, E. Y. Nikolskii, C. A. Bertulani, S. Fukuda, T. Kobayashi, E. A. Kuzmin, S. Momota, B. G. Novatskii, A. A. Ogloblin, and E. A. A. Ozawa, Nucl. Phys. **A617**, 45 (1997).

[34] M. El-Azab Farid and M. A. Hassanain, Nucl. Phys. **A697**, 183 (2002).

[35] D. T. Khoa (private communication).

[36] S. Gupta and K. Murthy, Z. Phys. A **307**, 187 (1982).

[37] H. Uberall, *Electron Scattering from Complex Nuclei* (Academic Press, New York, 1971).

[38] M. N. Harakeh and A. E. L. Dieperink, Phys. Rev. C **23**, 2329 (1981).

[39] D. H. Youngblood, Y.-W. Lui, and H. L. Clark, Phys. Rev. C **65**, 034302 (2002).

[40] R. Klein, P. Grabmayr, Y. Kawazoe, G. J. Wagner, J. Friedrich, and N. Voegler, Nuovo Cimento A **76**, 369 (1983).

[41] R. P. Singhal, S. W. Brain, C. S. Curran, W. A. Gillespie, A. Johnston, E. W. Lees, and A. G. Slight, J. Phys. G **1**, 558 (1975).

[42] S. Raman, C. W. Nestor, and P. Tikkanen, At. Data Nucl. Data Tables **78**, 1 (2001).

[43] T. Kibédi and R. H. Spear, At. Data Nucl. Data Tables **80**, 35 (2002).